Parametric Response Mapping as an Indicator of Bronchiolitis Obliterans Syndrome after Hematopoietic Stem Cell Transplantation

Galban, Craig J.; Boes, Jennifer L.; Bule, Maria; Kitko, Carrie L.; Couriel, Daniel R.; Johnson, Timothy D.; Lama, Vihba; Telenga, Eef D.; van den Berge, Maarten; Rehemtulla, Alnawaz

Published in:
Biology of Blood and Marrow Transplantation

DOI:
10.1016/j.bbmt.2014.06.014

Publication date:
2014

Biol Blood Marrow Transplant 20 (2014) 1592–1598

Biology of Blood and Marrow Transplantation

journal homepage: www.bbmt.org

ASBMT American Society for Blood and Marrow Transplantation

Parametric Response Mapping as an Indicator of Bronchiolitis Obliterans Syndrome after Hematopoietic Stem Cell Transplantation

Craig J. Galbán [1,*], Jennifer L. Boes [1], Maria Bule [1], Carrie L. Kitko [2,3], Daniel R. Couriel [2,4], Timothy D. Johnson [5], Vihba Lama [4], Eef D. Telenga [6], Maarten van den Berge [6], Alnawaz Rehemtulla [7], Ella A. Kazerooni [1], Michael J. Ponkowski [2], Brian D. Ross [1], Gregory A. Yanik [2,3,4]

[1] *Department of Radiology, University of Michigan, Ann Arbor, Michigan*
[2] *Blood and Marrow Transplant Program, University of Michigan, Ann Arbor, Michigan*
[3] *Department of Pediatrics and Communicable Diseases, University of Michigan, Ann Arbor, Michigan*
[4] *Department of Internal Medicine, University of Michigan, Ann Arbor, Michigan*
[5] *Department of Biostatistics, University of Michigan, Ann Arbor, Michigan*
[6] *Department of Pulmonary Diseases, University of Groningen, University Medical Center Groningen, Groningen, the Netherlands*
[7] *Department of Radiation Oncology, University of Michigan, Ann Arbor, Michigan*

Article history:
Received 20 March 2014
Accepted 10 June 2014

Key Words:
Bronchiolitis obliterans syndrome
Pulmonary
Transplantation

A B S T R A C T

The management of bronchiolitis obliterans syndrome (BOS) after hematopoietic cell transplantation presents many challenges, both diagnostically and therapeutically. We developed a computed tomography (CT) voxel-wise methodology termed parametric response mapping (PRM) that quantifies normal parenchyma, functional small airway disease (PRM^{fSAD}), emphysema, and parenchymal disease as relative lung volumes. We now investigate the use of PRM as an imaging biomarker in the diagnosis of BOS. PRM was applied to CT data from 4 patient cohorts: acute infection (n = 11), BOS at onset (n = 34), BOS plus infection (n = 9), and age-matched, nontransplant control subjects (n = 23). Pulmonary function tests and bronchoalveolar lavage were used for group classification. Mean values for PRM^{fSAD} were significantly greater in patients with BOS (38% ± 2%) when compared with those with infection alone (17% ± 4%, $P < .0001$) and age-matched control subjects (8.4% ± 1%, $P < .0001$). Patients with BOS had similar PRM^{fSAD} profiles, whether a concurrent infection was present or not. An optimal cut-point for PRM^{fSAD} of 28% of the total lung volume was identified, with values >28% highly indicative of BOS occurrence. PRM may provide a major advance in our ability to identify the small airway obstruction that characterizes BOS, even in the presence of concurrent infection.

INTRODUCTION

Pulmonary complications, both infectious and noninfectious, are a common cause of morbidity and mortality after hematopoietic cell transplantation (HCT). Within this context, bronchiolitis obliterans syndrome (BOS) remains particularly problematic, characterized clinically by fixed airflow obstruction of small airways and pathologically by progressive circumferential fibrosis of terminal bronchioles. BOS is extremely heterogeneous in its presentation, due in part to the nonuniform diagnostic criteria historically used to define the condition [1–3]. The development of National Institutes of Health consensus criteria (NIH-CC) over the past decade has been a major advance in our recognition and categorization of the disorder [2,4]. NIH-CC–defined clinical parameters for the diagnosis of BOS depend on a combination of clinical and radiographic findings, including diminished forced expiratory volumes in 1 second (FEV_1), evidence of air trapping on high-resolution computed tomography (HRCT), the absence of active pulmonary infection, and the presence of chronic graft-versus-host disease in another organ.

Using the NIH-CC definition, the criteria for BOS are often not met until a patient exhibits significant airway obstruction, with FEV_1 values typically less than 60% predicted at the defined onset [3,5]. Once present, the prognosis of affected patients is poor, with 5-year overall survival < 20% [5]. Therapeutic options for BOS are minimal, with responses measured as disease stabilization rather than functional

Financial disclosure: See Acknowledgments on page 1598.
* Correspondence and reprint requests: Craig J. Galbán, PhD, Assistant Professor, Department of Radiology, University of Michigan, BSRB, Room D206, 109 Zina Pitcher Place, Ann Arbor, MI 48109-2200.
E-mail address: cgalban@med.umich.edu (C.J. Galbán).

1083-8791/$ – see front matter © 2014 American Society for Blood and Marrow Transplantation.
http://dx.doi.org/10.1016/j.bbmt.2014.06.014

improvement [6,7]. Early recognition of the disorder, before the development of irreversible airway changes, may potentially lead to improvements in therapeutic responses and overall survival.

The parametric response mapping (PRM) technique has been developed at our center as a quantitative imaging biomarker for the assessment of obstructive lung disease. PRM is a voxel-based approach that provides detailed information on disease phenotype otherwise unattainable by conventional CT-based quantitative measures. Using biphasic (inspiratory and expiratory) HRCT, PRM is able to determine the severity, phenotype, and spatial heterogeneity of the pulmonary pathology using a methodology distinct from other CT-based measures [8–11]. PRM was first demonstrated on HRCT data from patients with chronic obstructive pulmonary disease, allowing quantification of the degree of functional small airway disease (fSAD) and emphysematous changes in relation to normal lung parenchyma [8]. Commonly used CT metrics for the diagnosis of lung disease have historically used tissue volumetric summary statistics of lung fields, including the mean lung density. PRM, however, classifies local variations in lung function based on a voxel-by-voxel comparison of lung attenuation changes from coregistered inspiratory and expiratory CT scans, providing both global and localized evaluations of lung pathology.

We now report on the application of PRM to patients with BOS after HCT, specifically adapted to quantify the relative contribution of fSAD in affected individuals irrespective of the presence of acute infection. A comparison of PRM in patients with BOS, at the time of initial diagnosis of BOS (based on NIH-CC) and during episodes of secondary infection, is now examined.

METHODS

Retrospective clinical data, pulmonary function analysis, and HRCT images at inspiration and expiration were obtained from 3 groups of HCT recipients at the University of Michigan Medical Center: group 1, infection, no BOS; group 2, BOS, no infection; and group 3, BOS, with infection. Group 1 patients were early post-HCT (<120 days), with an acute infectious pneumonitis and no clinical or radiographic features of BOS. Group 2 patients were selected at the time of NIH-CC–defined onset of BOS, without active pulmonary infection. Group 3 patients previously met the NIH-CC for BOS but now exhibited an infectious pneumonitis.

Bronchoalveolar lavage (BAL) studies, including BAL special stains, PCR assays for viral pathogens, and cultures for bacteria, fungi, viruses, and mycobacteria, were performed to establish the presence (or absence) of an infectious pneumonitis in patients in all groups. Pulmonary function tests (PFTs) including measurements of FEV_1, forced vital capacity (FVC), FEV_1/FVC ratio, residual volume, and lung diffusion capacity were obtained, with measurements expressed as percent predicted values. Modified NIH-CC were required to establish the diagnosis of BOS, including a $FEV_1 < 75\%$ predicted, signs of obstructive airway disease (FEV_1/FVC ratio <.7, residual volume >120% predicted, or evidence of air trapping on HRCT), absence of infection, and the presence of chronic graft-versus-host disease in another organ [4]. NIH lung function scores were determined, based on published methodology [4].

Bronchoscopy was performed within 14 days (group 1) or 28 days (groups 2 and 3) from the defined HRCT. PFTs were performed within 28 days of the HRCT in group 2 and 3 patients. Paired PFTs and HRCT were not available in group 1 patients, given the early post-transplant time course of this group. FEV_1, FEV_1/FVC, and lung diffusion capacity were acquired as part of the study design and analyzed in this study. In addition, a single case from group 2 was identified as having 5 interval CT examinations. Data were analyzed and presented to demonstrate the use of PRM to monitor pulmonary complications and disease progression. All transplant subjects signed an institutional review board–approved informed consent for data collection and analysis.

Additional age-matched, nontransplant, healthy subjects (group 4) were analyzed for this study to serve as negative control subjects (n = 23). These subjects, accrued as part of a separate clinical trial at the University Medical Center Groningen (NORM Study, NCT00848406), were individuals >40 years of age who did not smoke during the last year and had <.5 pack years smoking history. Pulmonary function measurements (FEV_1 and FEV_1/FVC) were acquired in all age-matched control subjects.

Parametric Response Mapping

The PRM method consists of 3 key steps: image acquisition, image processing, and voxel classification (Figure 1) [8].

Image acquisition

Internal CT data at the University of Michigan were obtained as whole lung volumetric CT scans at full inspiration (total lung capacity) and incremental scans at relaxed expiration (functional residual capacity) on GE scanners (GE Healthcare, Little Chalfont, UK) and reconstructed using a bone reconstruction kernel. Slice thicknesses were 1.25 mm for all scans, with slice numbers on average around 220 for inspiration scans and around 15 for expiration scans. All CT scans were linearly Hounsfield unit (HU)-corrected based on aortic blood (50 HU) and central air (−1000 HU) as described previously [12].

NORM Study CT data (for control subjects) were obtained as whole lung volumetric acquisitions both at full inspiration and forced expiration (residual volume) on a Somatom scanner (Siemens, Munich, Germany) with 1-mm slice thickness and a reconstruction index of .7 mm. A standard kernel (B30f) was used for image reconstruction. HU values of aortic blood (37 HU) and central air (−995 HU) were determined to check for scanner drift on all NORM data. All data were found to have negligible drift; as such, no HU corrections were performed.

Image processing

Image processing consisted of lung parenchymal segmentation followed by deformable volumetric registration, which spatially aligns the inspiration scan to the expiration scan such that both share the same spatial geometry. The lungs from expiratory CT scans acquired at the University of Michigan were segmented from the surrounding anatomy (ie, bronchus, heart, and chest wall) using in-house algorithms developed in a mathematical programming language (Matlab, Natick, MA). User verification and manual corrections were applied as necessary. Whole lung volumetric inspiration data were registered to the interval expiration data, allowing presentation of the PRMs. Inspiratory scans were coregistered to expiratory scans for all subjects and time points. Image registration was performed using a cost function of mutual information and thin-plate spline warping deformations [13]. Upon completion of image registration, the images share the same geometric space. Each voxel, the smallest unit of volume in a 3-dimensional image data set, consisted of a pair of HU values: 1 HU value at inspiration and 1 HU value at expiration. For reference, air and water attenuation values are −1000 and 0 HU, respectively.

The NORM trial acquired whole lung volumetric CT scans at both inspiration and expiration, with CT data processed by our group as described above. One distinction between the CT scans from the NORM trial and CT scans from group 1, 2, and 3 subjects was the direction of scan registration (geometric alignment), given differences in spatial arrangements between inspiratory and expiratory views. In the NORM Study, expiration scans were registered (aligned) to the inspiration scans [8], whereas CT scans for group 1, 2, and 3 subjects did the converse, aligning the inspiratory scans with the expiration scans.

Voxel classification

Classification of the voxels from attenuation maps into discrete zones allows quantification of normal lung parenchyma, fSAD, emphysema, and parenchymal disease characteristic of infection (Figure 1, Table 1). Three thresholds are used to classify individual voxels into 1 of 4 categories with the following color codes: emphysema (red voxels), fSAD (yellow voxels), normal parenchyma (green voxels), and parenchymal disease (purple voxels). Voxels with HU values less than −950 on the inspiration scan and at least −856 on the expiration scan have been identified previously as having a weak correlation to pulmonary function (ie, FEV_1) [8]. As such, no analysis was performed on this measure. In addition, parenchymal tissue with voxel values above −500 HU on the inspiration scan were not analyzed in this study. Global PRM measures were calculated by normalizing the sum of all voxels within a classification by the total lung volume, which include all parenchymal voxels over the full range of HU. The nomenclature of these measures for normal lung parenchyma, fSAD, emphysema, and parenchymal disease were PRM^{Normal}, PRM^{fSAD}, PRM^{Emph}, and PRM^{PD}, respectively.

Thresholds of −950 HU and −856 HU on the inspiration and expiration scans, respectively, were defined as specified by the COPDGene study [14]. The upper limit on the inspiration CT (−810 HU) was determined using inspiration CT scans from the age-matched control subjects (group 4; n = 23) obtained from the NORM Study. Briefly, the CT lung density data were normalized by taking their natural logarithm. A bi-Gaussian fit was performed on the normalized CT data and the 95% confidence interval (1.96 × standard deviation) of the principle peak that resides in a range of −1000 to −500 was determined.

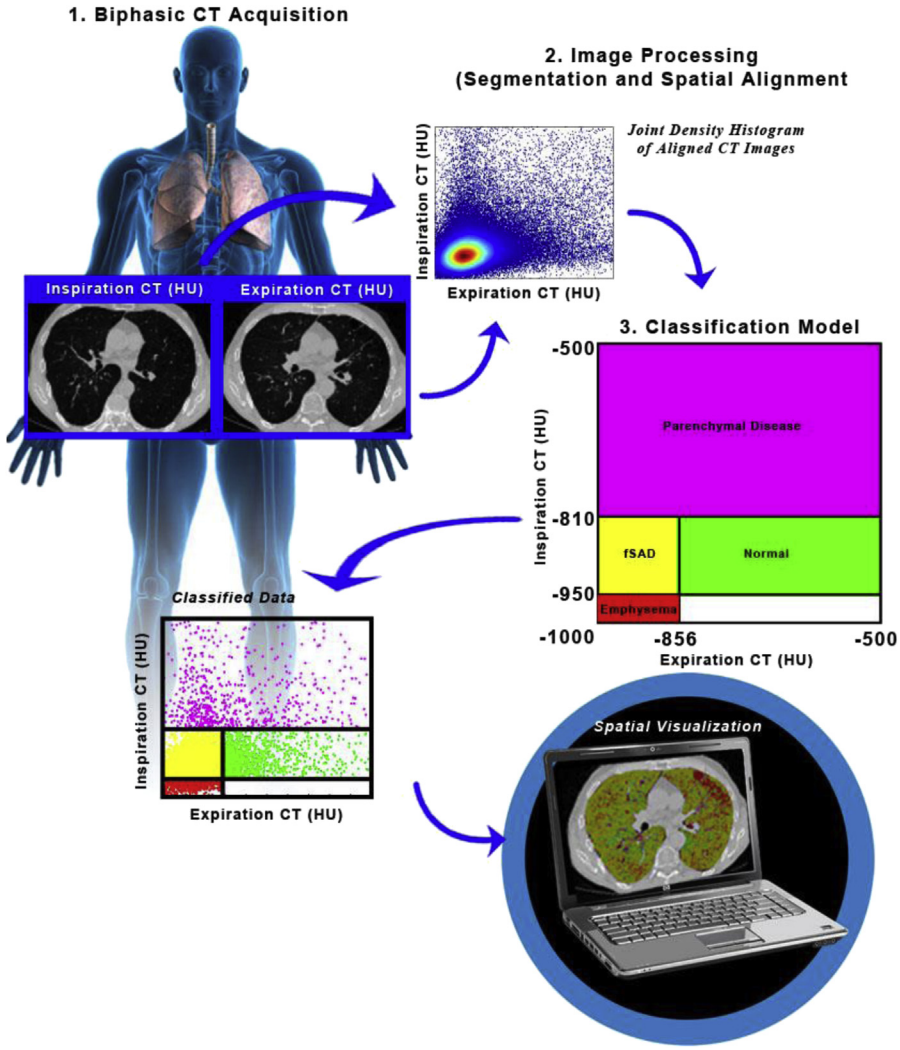

Figure 1. Schematic diagram of the PRM workflow.

Statistical Analysis

Group comparisons were determined for PRM and PFT measures using an analysis of variance controlling for multiple comparisons using a Bonferroni post-hoc test. A receiver operating characteristic (ROC) analysis was performed for correlation of PRM^{fSAD} with subjects diagnosed with BOS. Only subjects from group 1 (infection alone; n = 11) and group 2 (BOS alone; n = 34) were used in this analysis. A more rigorous evaluation of PRM^{fSAD} as an indicator of BOS was performed using a discriminant analysis with leave-one out cross-validation using groups 1 and 2. The discriminant analysis was used to generate a predictive model for classifying subjects in groups 1 and 2 into 2 predicted groups. An additional ROC analysis was then applied using PRM^{fSAD} as an independent variable and the new predicted dichotomized variable to determine an optimal cut-off for indicating BOS. Results were considered statistically significant at the 2-sided 5% comparison-wise significance level ($P < .05$). All data are presented as the mean ± SEM. All statistical computations were performed with a statistical software package (IBM SPSS Statistics, v. 21, Armonk, NY).

RESULTS

CT and PFT data were acquired from 77 patients, including 54 patients who underwent HCT at the University of Michigan and 23 control (nontransplant) subjects (Table 2). Group 1 subjects (infection, n = 11) underwent CT a median of 63 days (range, 19 to 109) post-HCT. Infections in group 1 subjects included aspergillus (n = 5), rhizopus (n = 2), fusarium (n = 1), cytomegalovirus (n = 1), *Moraxella* (n = 1), herpes hominis virus 6 (n = 1), and *Pneumocystis jirovecii* (n = 1), with multiple pathogens identified in 2 patients. Group 2 subjects (BOS, no infection) were selected at the time the NIH-CC for BOS were met (n = 34), undergoing CT a median of 638 days (range, 199 to 1545) post-HCT. Group 3 subjects (BOS + infection) (n = 9) all had previously met the NIH-CC for BOS but now exhibited an infectious pneumonitis, undergoing CT a median of 970 days (range, 259 to 3940) post-HCT. Infections in group 3 subjects included aspergillus (n = 5), *Pseudomonas* (n = 2), and nontuberculi *Mycobacterium* species (n = 2). Infections in this group were typically subacute in nature, without acute infectious symptomatology (fevers, chest pain, productive cough).

Table 1
Classification Schema, Based on Attenuation Maps

	PRM^{Emph}	PRM^{fSAD}	PRM^{PD}	PRM^{Normal}
Inspiration	$-1000 \leq$ to < -950 HU	$-950 \leq$ to < -810 HU	$-810 \leq$ to < -500 HU	$-950 \leq$ to < -810 HU
Expiration	$-1000 \leq$ to < -856 HU	$-1000 \leq$ to < -857 HU	$-1000 \leq$ to < -500 HU	$-856 \leq$ to < -500 HU

Table 2
Demographics

	Group 1 (Infection)	Group 2 (BOS)	Group 3 (BOS + Infection)	Control Subjects
Total patients	11	34	9	23
Age, yr				
Median	58	54	53	57
Range	38-68	12-69	30-69	44-73
Gender				
Males/Females	10/1	16/18	3/6	16/7
Disease				NA*
AML/MDS	3	21	4	
ALL	1	5	0	
Lymphomas	5	2	3	
Myeloma	2	2	2	
CML	0	4	0	
Days post-transplant				NA
Median	63	638	970	
Range	19-109	199-1545	259-3940	
PFT†				
FVC (median %)	NA‡	72	64	111
FEV_1 (median %)	NA	46	38	119
Lung diffusion capacity (median %)	NA	54	49	NA
NIH lung function scores§				
Median	NA	8	9	NA
Range	NA	3-12	5-12	

AML indicates acute myelogenous leukemia; MDS, myelodysplastic syndrome; ALL, acute lymphoblastic leukemia; CML, chronic myelogenous leukemia.

* Control subjects were healthy nontransplant subjects, nonsmokers, with no underlying malignancy.

† Values are expressed as percent predicted.

‡ PFTs were not obtained at the time of HRCT for group 1 patients.

§ NIH lung function scores per Filipovich [4].

Group 4 patients consisted of age-matched, nontransplant control subjects, with FVC and FEV_1 values above 100% predicted in these subjects.

The ability of PRM to characterize pulmonary pathology is demonstrated in representative axial PRM images from age-matched control subjects (Figure 2A and 3) individuals with pulmonary complications after HCT, including an acute infectious pneumonitis (Figure 2B), BOS at NIH-CC–defined onset (Figure 2C), and BOS with concurrent infection (Figure 2D). PRM classified voxels as parenchymal disease (PRM^{PD}, purple in Figure 2B,D) with relative volumes approximately 30% of the total lung volume in these figures. Subjects diagnosed with BOS, irrespective of the presence of infection, were identified as having extensive nonemphysematous air trapping as indicated by PRM^{fSAD} (yellow in Figure 2C,D). Parenchyma in a healthy control subject was identified as being normal by PRM (PRM^{Normal}, green Figure 2A).

PRM from the control subjects were similar to those observed in our previously published work [8]. In contrast, reduced levels of normal lung parenchyma (PRM^{Normal}) were noted for all 3 transplant groups ($P < .0001$) (Figure 3). Mean PRM^{fSAD} were increased in subjects with BOS, in both group 2 ($38\% \pm 2\%$) and group 3 ($35\% \pm 3\%$). The mean PRM^{fSAD} for group 2 and 3 subjects was significantly higher than group 1 subjects ($17\% \pm 4\%$, $P < .01$) and age-matched control subjects ($8.4\% \pm 1\%$, $P < .0001$). There was no significant difference in mean PRM^{fSAD} between subjects in groups 2 and 3, $P =$ NS. Mean PRM^{PD} values were $17\% \pm 2\%$ in group 2 (BOS, no infection) and $11\% \pm 2\%$ in age-matched control subjects ($P < .001$). Although the mean PRM^{PD} was higher in group 1

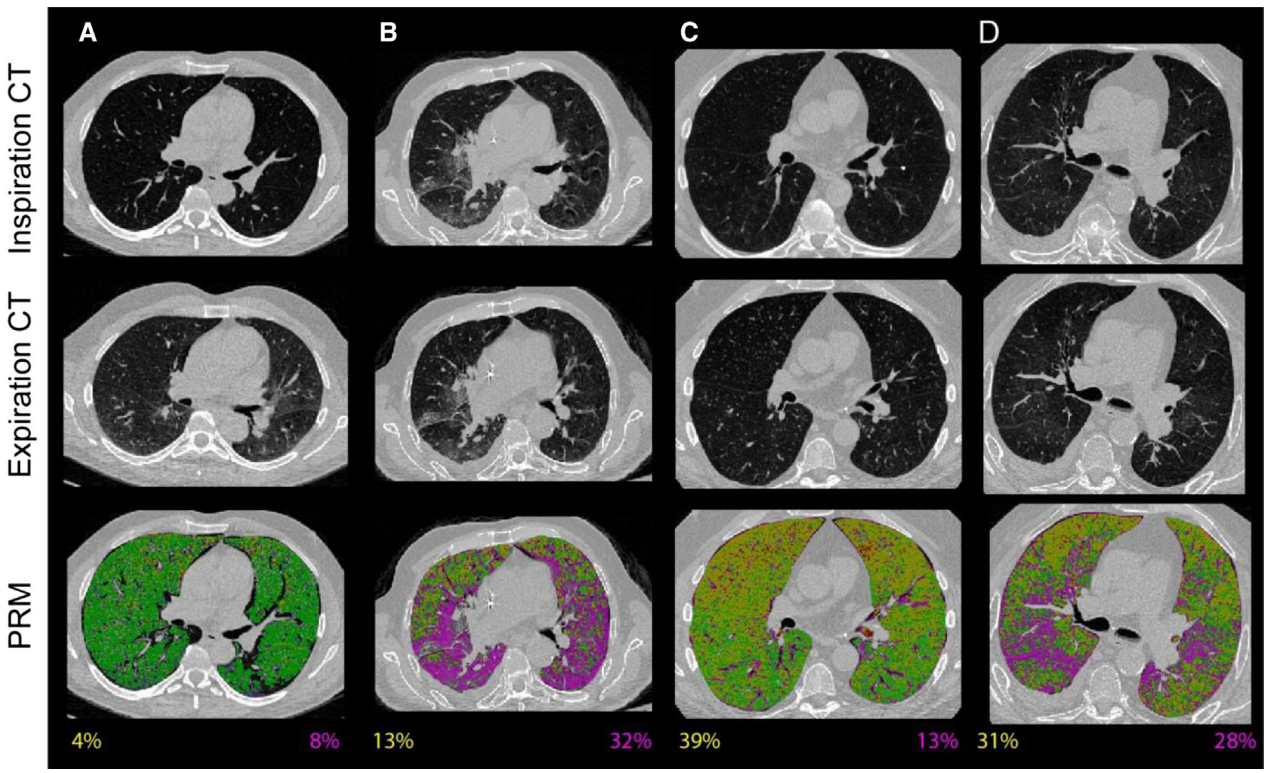

Figure 2. Pulmonary complications identified by PRM. Normal lung tissue is denoted green (PRM^{Normal}), functional small airway disease yellow (PRM^{fSAD}), emphysematous changes red (PRM^{Emph}), and parenchymal disease purple (PRM^{PD}). PRM^{fSAD} and PRM^{PD} values are provided at the bottom of PRM images (values are color coded to disease component). (A) Healthy age-matched, nontransplant control subjects. (B) Fungal pneumonitis, 61 days post-HCT. (C) BOS at NIH-CC–defined onset, 448 days post-HCT. No concurrent infection present. (D) *Pseudomonas* pneumonitis in a patient with previously documented BOS, now 447 days post-HCT.

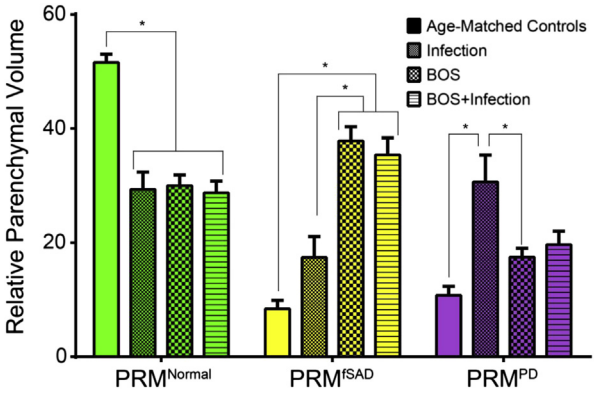

Figure 3. Group comparisons in pulmonary function measures and PRM. Bar plots are used to present the group differences observed in PRM measurements, PRM^{Normal}, PRM^{fSAD}, and PRM^{PD}. Statistical significance was assessed at $P < .05$ and denoted by an asterisk. Data are presented as means ± SEM.

(30% ± 4%) versus group 3 (20% ± 2%) patients, the difference was not significant, $P = .08$. There was also no significant difference in the level of PRM^{PD} between group 2 and group 3 subjects, potentially due to the subacute nature of the infections in the group 3 patients. PRM^{Emph}, a measure for severe emphysematous changes, was <5% for all 3 subject groups. Significant differences in mean PRM^{Emph} levels were only observed between group 1 and 2 patients, with mean PRM^{Emph} values of .3% and 4.0% respectively, $P = .04$.

We analyzed the predictive potential of PRM^{fSAD} in identifying subjects with BOS (group 2; n = 34) from those with acute pulmonary infection (group 1; n = 11). We first used a ROC analysis to correlate PRM^{fSAD} with the likelihood that an individual would have BOS. PRM^{fSAD} was found to significantly identify BOS with an area under the curve of .861 ($P < .001$) and 95% confidence intervals of .743 and .979. We next performed a discriminant analysis with leave-one out cross-validation that provided a more rigorous test of PRM^{fSAD} as an indicator of BOS. Through the discriminant analysis, we again found PRM^{fSAD} to be a significant predictor of BOS with sensitivity and specificity of .76 and .72, respectively ($P < .0001$). Of all cross-validated grouped cases, 75% were correctly classified. To determine an optimal cut-off, a ROC analysis of PRM^{fSAD} using the newly classified data from our discriminant analysis generated an optimal PRM^{fSAD} cut-off of 28% of the total lung volume, with values >28% indicative of BOS. This PRM^{fSAD} cut-point (>28%) remained a valid indicator of BOS, irrespective of the presence (or absence) of a concurrent infection.

Serial PRM Measurements

The potential ability of PRM to identify significant fSAD in patients, before fulfillment of the NIH-CC for BOS, is shown in Figure 4. In this patient, PRM imaging from a HRCT obtained 1 year post-HCT revealed PRM^{fSAD} of 41%, with 17% PRM^{PD}. The NIH-CC for BOS would not be fulfilled, however, until nearly 3 years post-HCT. During this same period, PRM^{fSAD} levels continued to increase, peaking at 3 years post-HCT at 65%, with PRM^{Normal} decreasing from 27% to 13% over the same time period. The subject subsequently underwent a lung allograft approximately 7 years post-HCT for management of his end-stage lung disease. As anticipated, PRM^{Normal}

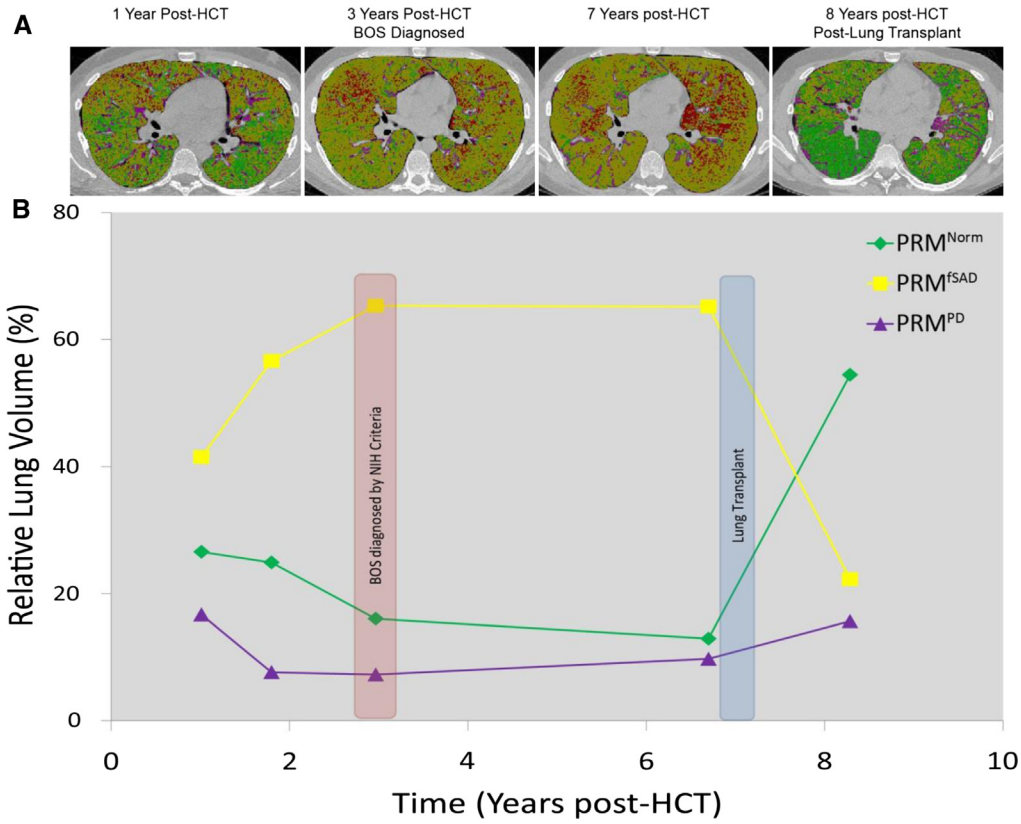

Figure 4. Onset and progression of BOS post-HCT in a single patient. (A) Representative PRM axial slices are provided at discrete time points after HCT. (B) Line plot with axes time (years) and PRM relative lung volumes (%) at various time points post-HCT.

values increased significantly after the lung allograft, from 13% to 54% of the total lung volume (Figure 4).

DISCUSSION

We demonstrate the utility of PRM, a voxel-based imaging technique applied to paired inspiratory and expiratory CT lung scans, to serve as a diagnostic index of fSAD after HCT. Elevated levels of PRM^{fSAD} were present in patients with BOS, even in the setting of concurrent pulmonary infection. An optimal cut-point for PRM^{fSAD} of 28% of the total lung volume was identified, with values >28% highly indicative of BOS. In addition, by retaining spatial information within the lung parenchyma, PRM provides a unified methodology that can simultaneously identify and quantify the extent of fSAD within the lungs. Quantitative PRM measures can be tracked temporally, providing real-time diagnostic information on the progression of fSAD that could be acted on by the treating physician.

BOS is currently defined by NIH-CC in which obstructive airway disease (by radiographic and spirometric parameters) plus absence of active lung infection are required to establish the diagnosis. The application of the NIH-CC can be challenging, given the frequent infectious complications that affected patients often exhibit post-HCT. Recurrent infections in this patient population hinder our diagnostic capabilities, with patients often meeting NIH-CC for BOS only after severe airflow abnormalities are already present. This is an important problem, because once a patient is diagnosed with BOS, overall survival is poor, <20% at 5 years [15]. The ability of PRM to identify significant elevations in fSAD, even in the setting of an active infection, may lead to earlier recognition of BOS and subsequent treatment interventions.

The role of PRM as an imaging biomarker for detection of BOS requires validation in larger case series and may ultimately complement known diagnostic markers for disease. A number of novel biomarkers for early BOS detection, including serologic and BAL fluid biomarkers, were recently reported in lung allograft and HCT recipients, including the glycoprotein YKL-40, hypoxia inducible-1α, and various metalloproteinases [16–18]. In lung allograft recipients, BAL fluid levels of IL-15, IL-17, TNF-α, and α_1-antitrypsin were predictive of BOS development in one report [17], with overexpression of IL-8, lung surfactant proteins A and D, and BAL fluid neutrophil levels predictive of BOS in other reports [18,19]. Noninvasive biomarkers, including measurement of fractional exhaled nitric oxide, may additionally serve a role in early BOS detection [20]. Given the heterogeneity of the disorder, with complexities in both diagnosis and management, a panel of both invasive and noninvasive biomarkers may be required for diagnosis and risk classification of patients.

The current study focuses on the application of PRM in patients with BOS after HCT. The study was not designed to examine PRM within specific infections or examine the role of PRM in other noninfectious pneumonitis post-HCT, including idiopathic pneumonia syndrome, restrictive lung disease, and cryptogenic organizing pneumonia. Fungal pathogens were the predominant pathogen in both group 1 (infection, no BOS) and group 3 (BOS, with infection) patients, with a paucity of bacterial ($n = 3$) and viral pneumonitis ($n = 2$) present within the study population. In addition, the current study did not find significant differences in fSAD levels between group 2 (BOS, no infection) and group 3 (BOS, with infection), both groups exhibiting >30% mean PRM^{fSAD}. This is an important finding to note, because increased levels of fSAD were thus present in patients with BOS, regardless if a concurrent infection were present or not.

BOS exhibits a wide spectrum of phenotypes, characterized by a lymphocytic bronchitis and small airway inflammation early in the clinical course, with subsequent fibrinous obliteration of bronchiolar lumen developing later in the disease [21,22]. The histologic changes are often heterogeneous in nature, with varying degrees of involvement within segments of individual lobes. Correlation of lung histology with PRM values was limited in the current trial, with surgical lung or transbronchial biopsies performed in only 6 of the 34 group 2 patients. The spatial information gathered by PRM may ultimately help clinicians identify (and target) optimal sites for biopsy and lavage during diagnostic bronchoscopic procedures.

Although CT is widely used for diagnosis and staging of various lung disorders, a lack of consensus has brought about various acquisition protocols and reconstruction algorithms between CT scanners. In general, the best clinical practice for the use of CT in diagnosing BOS is to use a well-calibrated HRCT and to apply consistent acquisition and reconstruction parameters. PRM may provide disparate results from multiple time-point CT examinations that do not take precautionary measures to avoid inconsistencies in acquisition and reconstruction parameters. Nevertheless, image post-processing can be performed to minimize fluctuations in HU values between similar CT examinations (eg, acquired at full inspiration, consistent lung histograms). We, and others, find that HU values can be corrected to minimize effects from scanner drift [12,23]. This procedure for correcting datasets allows the use of archival data in many cases. Even low-resolution interval expiration scan data produce reliable PRM results. Using a separate cohort of CT data, we determined that the insertion of gaps (maximum 10-mm gap) in whole lung volumetric expiration CT data only generated differences of 1.6% from the high-resolution (contiguous) PRM analysis (unpublished results, JLB, BDR, CJG, 2014). Nevertheless, HU-based measurements using widely spaced axial slices have the potential to misrepresent disease classification, particularly when the disease is spatially heterogeneous.

Other limitations in the current study must be addressed. The first is the retrospective nature of sample collection, resulting in the use of varying CT protocols on an interpatient basis. Despite the great care that was taken to minimize intrapatient variability in CT protocols and reconstruction algorithms, in some cases patient CT acquisitions and reconstruction algorithms varied slightly. As described previously, additional analyses were performed to investigate the sensitivity of PRM measurements to low-resolution interval expiration CT scans and reconstruction algorithms. In addition, we previously tested the effect of different registration directions on the PRM results. Again using a separate cohort of whole lung volumetric inspiration and expiration CT data, we found that registering to the expiration scans overestimates the amount of PRM^{fSAD} in absolute terms by approximately 5% when compared with PRM results from registrations to the inspiration scans (unpublished data, JLB, BDR, CJG, 2014). Although beyond the scope of this study, a more thorough analysis is necessary to fully ascertain the limits of the PRM analytical approach.

This is the first trial to investigate the role of PRM in characterizing BOS post-HCT. Many questions remain. Is there a more optimal PRM^{fSAD} cut-point for identifying BOS, one with a higher sensitivity and specificity than currently exhibited?

Can PRM provide earlier detection of BOS than standard spirometry, before any significant decline in FEV_1 or FEV_1/FVC? Can a PRM signature for BOS be validated in a multicenter trial, in which centers have applied varying CT acquisition techniques? Does a PRM signature exist for other pulmonary complications post-HCT, potentially differentiating infectious from noninfectious pulmonary complications? Ultimately, PRM requires testing in a multisite clinical trial consisting of highly characterized subjects with detailed longitudinal data collection, including spirometric measurements, to validate this work in both BOS and other post-transplant lung complications.

In conclusion, PRM provides a quantitative imaging analysis for patients with BOS after HCT, with elevated levels of fSAD present in affected patients. The ability for PRM to both quantify and spatially define the severity of lung airway disease in patients with BOS may serve as a major advance in the diagnosis and management of this disorder.

ACKNOWLEDGMENTS

The authors thank Ms. Verica Saveski and Ms. Sandra Klaus for their administrative assistance with this project.

Financial disclosure: Supported by the US National Institutes of Health research grants P50CA93990 and P01CA085878. J.L.B. is a recipient of support from the US National Institutes of Health training grant T32EB005172.

Conflict of interest statement: B.D.R. and C.J.G. have a financial interest in the underlying patented University of Michigan technology licensed to Imbio, LLC., a company in which B.D.R. and A.R. have a financial interest. There are no other conflicts of interest.

Authorship statement: C.J.G. designed and performed the research, analyzed data, and wrote the manuscript. J.L.B. processed and analyzed data and wrote the manuscript. M.B. processed and analyzed data. C.L.K. analyzed data and wrote the manuscript. D.R.C. analyzed data. T.D.J. performed statistical analysis. V.L. designed research. E.D.T. and M.V.D.B. provided data on control subjects. A.R. designed and performed the research. E.A.K. designed and performed the research and wrote the manuscript. M.P. collected clinical data on subjects. B.D.R. designed and performed the research. G.A.Y. designed the research, collected clinical data, analyzed data, and wrote the manuscript.

REFERENCES

1. Afessa B, Litzow MR, Tefferi A. Bronchiolitis obliterans and other late onset non-infectious pulmonary complications in hematopoietic stem cell transplantation. *Bone Marrow Transplant*. 2001;28:425-434.
2. Williams KM, Chien JW, Gladwin MT, Pavletic SZ. Bronchiolitis obliterans after allogeneic hematopoietic stem cell transplantation. *JAMA*. 2009;302:306-314.
3. Au BK, Au MA, Chien JW. Bronchiolitis obliterans syndrome epidemiology after allogeneic hematopoietic cell transplantation. *Biol Blood Marrow Transplant*. 2011;17:1072-1078.
4. Filipovich AH. Life-threatening hemophagocytic syndromes: current outcomes with hematopoietic stem cell transplantation. *Pediatr Transplant*. 2005;9(Suppl 7):87-91.
5. Chien JW, Duncan S, Williams KM, Pavletic SZ. Bronchiolitis obliterans syndrome after allogeneic hematopoietic stem cell transplantation-an increasingly recognized manifestation of chronic graft-versus-host disease. *Biol Blood Marrow Transplant*. 2010;16(1 Suppl):S106-S114.
6. Hildebrandt GC, Fazekas T, Lawitschka A, et al. Diagnosis and treatment of pulmonary chronic GVHD: report from the consensus conference on clinical practice in chronic GVHD. *Bone Marrow Transplant*. 2011;46:1283-1295.
7. Yanik G, Kitko C. Management of noninfectious lung injury following hematopoietic cell transplantation. *Curr Opin Oncol*. 2013;25:187-194.
8. Galban CJ, Han MK, Boes JL, et al. Computed tomography-based biomarker provides unique signature for diagnosis of COPD phenotypes and disease progression. *Nat Med*. 2012;18:1711-1715.
9. Gevenois PA, De Vuyst P, de Maertelaer V, et al. Comparison of computed density and microscopic morphometry in pulmonary emphysema. *Am J Respir Crit Care Med*. 1996;154:187-192.
10. Gorbunova V, Lol P, Ashraf H, et al. Weight preserving image registration for monitoring disease progression in lung CT. *Med Image Comput Comput Assist Interv*. 2008;11(Pt 2):863-870.
11. Matsuoka S, Kurihara Y, Yagihashi K, et al. Quantitative assessment of air trapping in chronic obstructive pulmonary disease using inspiratory and expiratory volumetric MDCT. *AJR Am J Roentgenol*. 2008;190:762-769.
12. Stoel BC, Stolk J. Optimization and standardization of lung densitometry in the assessment of pulmonary emphysema. *Invest Radiol*. 2004;39:681-688.
13. Meyer CR, Boes JL, Kim B, et al. Demonstration of accuracy and clinical versatility of mutual information for automatic multimodality image fusion using affine and thin-plate spline warped geometric deformations. *Medical Image Anal*. 1997;1:195-206.
14. Regan EA, Hokanson JE, Murphy JR, et al. Genetic epidemiology of COPD (COPDGene) study design. *COPD*. 2010;7:32-43.
15. Chien JW, Sakai M, Gooley TA, et al. Influence of oral beclomethasone dipropionate on early non-infectious pulmonary outcomes after allogeneic hematopoietic cell transplantation: results from two randomized trials. *Bone Marrow Transplant*. 2010;45:317-324.
16. Jaksch P, Taghavi S, Klepetko W, Salama M. Pretransplant serum human chitinase-like glycoprotein YKL-40 concentrations independently predict bronchiolitis obliterans development in lung transplant recipients. *J Thorac Cardiovasc Surg*. 2014;148:273-281.
17. Fisichella PM, Davis CS, Lowery E, et al. Aspiration, localized pulmonary inflammation, and predictors of early-onset bronchiolitis obliterans syndrome after lung transplantation. *J Am Coll Surg*. 2013;217:90-100. discussion 100-101.
18. Ditschkowski M, Elmaagacli AH, Koldehoff M, et al. Bronchiolitis obliterans after allogeneic hematopoietic SCT: further insight—new perspectives? *Bone Marrow Transplant*. 2013;48:1224-1229.
19. Kennedy VE, Todd JL, Palmer SM. Bronchoalveolar lavage as a tool to predict, diagnose and understand bronchiolitis obliterans syndrome. *Am J Transplant*. 2013;13:552-561.
20. Neurohr C, Huppmann P, Leuschner S, et al. Usefulness of exhaled nitric oxide to guide risk stratification for bronchiolitis obliterans syndrome after lung transplantation. *Am J Transplant*. 2011;11:129-137.
21. Urbanski SJ, Kossakowska AE, Curtis J, et al. Idiopathic small airways pathology in patients with graft-versus-host disease following allogeneic bone marrow transplantation. *Am J Surg Pathol*. 1987;11:965.
22. Cooke KR, Yanik G. Lung injury following hematopoietic stem cell transplantation. In: Appelbaum FR, Forman SJ, Negrin RS, Blume KG, editors. *Thomas' hematopoietic cell transplantation*, 4th ed. West Sussex, UK: Wiley-Blackwell; 2009. p. 1456-1472.
23. Tanabe N, Muro S, Hirai T, et al. Impact of exacerbations on emphysema progression in chronic obstructive pulmonary disease. *Am J Respir Crit Care Med*. 2011;183:1653-1659.